Uluç Saranli

Department of Electrical Engineering and Computer Science
University of Michigan
Ann Arbor, MI 48109-2110, USA

Martin Buehler

Center for Intelligent Machines
McGill University
Montreal, Québec, Canada, H3A 2A7

Daniel E. Koditschek

Department of Electrical Engineering and Computer Science
University of Michigan
Ann Arbor, MI 48109-2110, USA

RHex: A Simple and Highly Mobile Hexapod Robot

Abstract

In this paper, the authors describe the design and control of RHex, a power autonomous, untethered, compliant-legged hexapod robot. RHex has only six actuators—one motor located at each hip— achieving mechanical simplicity that promotes reliable and robust operation in real-world tasks. Empirically stable and highly maneuverable locomotion arises from a very simple clock-driven, open-loop tripod gait. The legs rotate full circle, thereby preventing the common problem of toe stubbing in the protraction (swing) phase. An extensive suite of experimental results documents the robot's significant "intrinsic mobility"—the traversal of rugged, broken, and obstacle-ridden ground without any terrain sensing or actively controlled adaptation. RHex achieves fast and robust forward locomotion traveling at speeds up to one body length per second and traversing height variations well exceeding its body clearance.

KEY WORDS—legged locomotion, hexapod robot, clock driven, mobility, autonomy, biomimesis

1. Introduction

In this paper, we report on a power autonomous legged vehicle, RHex (Fig. 1), that easily traverses terrain approaching the complexity and diversity of the natural landscape. Table 1 substantiates in part our belief that this machine breaks the speed record to date for power autonomous legged robot locomotion over uneven terrain by a considerable margin.[1]

1. Unfortunately, there is not enough performance detail documented in the published robotics literature to unconditionally establish this claim. To the best of our knowledge, the very few robots that have been demonstrated to negotiate uneven terrain at all travel at speeds far less than those we report here.

RHex travels at speeds approaching one body length per second over height variations exceeding its body clearance (see Extensions 1[2] and 2). Moreover, RHex does not make unrealistically high demands of its limited energy supply (two 12-V sealed lead-acid batteries in series, rated at 2.2 Ah): at the time of this writing (spring 2000), RHex achieves sustained locomotion at maximum speed under power autonomous operation for more than 15 minutes.

The robot's design consists of a rigid body with six compliant legs, each possessing only one independently actuated revolute degree of freedom. The attachment points of the legs as well as the joint orientations are all fixed relative to the body. The use of spoked wheels (or even highly treaded wheels) is of course an old idea. Comparable morphologies such as rimless wheels (Coleman, Chatterjee, and Ruina 1997) or single-spoked wheels (Honeywell 1920) have been previously proposed for mobile platforms. Some compliant legged designs have been proposed for toys (Grimm 1958), and some rigid, rimless wheel designs have actually been commercialized by the toy industry (Mattel's Major Matt Mason's No. 6304 Space Crawler). However, the major difference between a single leg and a wheel with more than two spokes arises from the far greater range of control over the ground reaction forces (GRF) that the former affords relative to the latter. Wheels afford control primarily over the horizontal component of the GRF (assuming flat ground) through friction, incurring an essentially uncontrolled concomitant vertical component. In contrast, a leg, by admitting selection over the angle of contact, yields a GRF whose direction as well as magnitude may be substantially controlled. As soon as multiple spokes are added, the

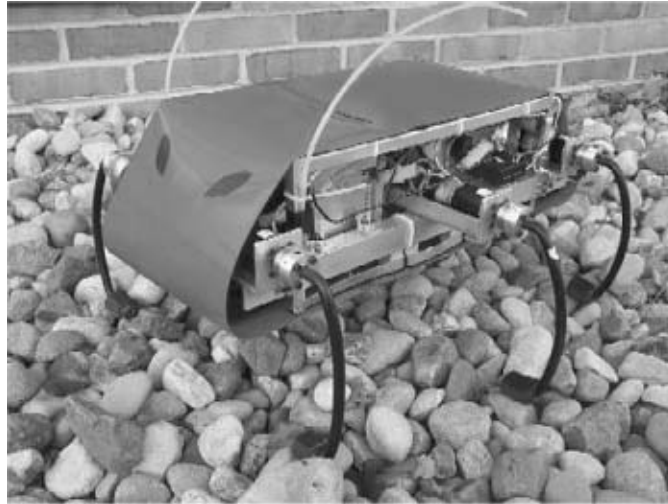2. Please see the Index to Multimedia Extensions at the end of this article.

Fig. 1. RHex experimental platform (www.RHex.net).

Table 1. Summary of Published Performance Reports: Hexapedal Robot

Name	L (m)[b]	M (kg)[b]	V (m/s)[b]	V/L
Case Western Robot II (Chiel et al. 1992)	0.5	1	0.083	0.16
Dante II (Bares and Wettergreen 1999)	3	770	0.017	0.006
Atilla[a] (Angle 1991)	0.36	2.5	0.03	0.083
Genghis[a] (Angle 1989)	0.39	1.8	0.038	0.097
Adaptive Suspension Vehicle[a] (Pugh et al. 1990)	5	3200	1.1	0.22
Boadicea (Binnard 1995)	0.5	4.9	0.11	0.22
Sprawlita (Clark et al. 2001)	0.17	0.27	0.42	2.5
RHex[a]	0.53	7	0.55	1.04

a. Power autonomous.

b. L = body length, M = robot mass, V = maximum speed.

interspoke angle restricts the range of contact angles, thereby diminishing control affordance. Our design preserves the possibility of achieving full GRF range while adding the virtues of tuned compliance, heretofore associated only with wheels.

The closest extant robots, one significant source of inspiration for the RHex design, are Buehler's (Buehler et al. 1998; Buehler et al. 1999; Papadopoulos and Buehler 2000) Scout class quadrupeds (www.cim.mcgill.ca/~arlweb), which also feature compliant legs and reduce mechanical complexity by the restriction of one actuator per leg.[3] The central difference with respect to this design is the possibility of recirculating (i.e., treating the singly actuated leg as a single-spoked "rimless wheel"). A second key design influence whose careful consideration exceeds the scope of this paper arises from biomechanics. R. J. Full's video of a *Blaberus* cockroach racing seemingly effortlessly over the rough surface illustrated in Figure 2 was shown at the spring 1998 meeting of the National

Science Foundation Institute for Mathematics and Its Applications, motivating and initiating the development of RHex. The present design may be seen as instantiating the notion of a "preflex" (Brown and Loeb 2000)—implemented here in the clock-driven, mechanically self-stabilizing, compliant sprawled-posture mechanics that Full et al. (1998) proposed.[4] The notion of a clock-driven mechanism arises in our choice of control strategies, deriving appropriate advantage of RHex's mechanical design. At the time of this writing, RHex operates by tracking (via local proportional-derivative [PD] control) at each hip joint a copy of the reference trajectory depicted in Figure 4 that enforces an alternating tripod gait in an otherwise open-loop manner. The two tripods are driven in relative antiphase. The three legs of a tripod are driven simultaneously through a slow "retraction" phase, putatively corresponding to ground contact, followed by a fast "protraction" phase designed to recirculate the legs away from the ground around the

---

3. Scout II travels at just under two body lengths per second but traverses only level ground.

4. See Altendorfer et al. 2000 for a technical discussion of some aspects relating the bioinspiration behind this design to its performance.

Fig. 2. Comparative views of locomotion in the rough: the cockroach *Blaberus discoidalis* (top photo, courtesy of R. J. Full) runs at 3.7 body lengths ($\sim$24 cm) per second (Full et al. 1998), whereas RHex (bottom photo) presently runs at only one body length ($\sim$50 cm) per second over comparably scaled broken terrain (see Extensions 3 and 4).

Fig. 3. Compliant hexapod design.

axle just in time to reach the next retraction phase, putatively as the opposing tripod begins its protraction by rotating away from ground contact. No design we are aware of has heretofore incorporated this combination of controller simplicity, leg compliance, limited actuation, and overall morphology, and no previously implemented legged vehicle has achieved the performance we now report.

Table 1 (modeled on but extended from Binnard 1995) summarizes performance data of previous hexapedal vehicles for which we are aware of documented performance, with citations to refereed publications. It would be of considerable interest to compare across a broader range of machines. Unfortunately, it is not straightforward to normalize against morphology. For example, "body lengths per second" is clearly not an appropriately normalized measure of bipedal speed. We look forward to the eventual adoption of appropriately general performance metrics for legged locomotion within the robotics research community. For the present, it seems most useful to compare the design of RHex with some of its more closely related forebears.
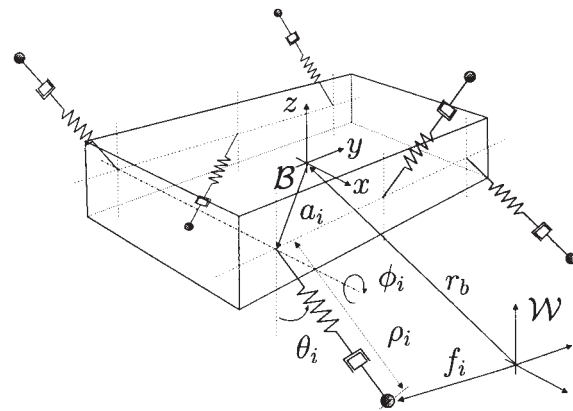
One of the better documented, faster power autonomous hexapods is the Ohio State University Adaptive Suspension Vehicle (ASV), which was designed to operate in the statically stable regime. The deleterious consequences of design complexity have been observed in Dante II (Bares and Wettergreen 1999), a tethered hexapod whose exposure to severe environmental conditions has apparently been the most extreme of any robot yet documented in the archival literature. On a smaller scale, there have been many platforms inspired by insect locomotion (Angle 1989, 1991; Binnard 1995), all designed for statically stable gaits. Their speeds were thus limited even though their design afforded greater kinematic freedom over limb motions. A notable exception in the smaller scale is Sprawlita (Clark et al. 2001), a tethered hexapod that can achieve a very impressive 2.5 body lengths per second locomotion speed as a result of its careful (compliant leg) design and construction (offboard pneumatic actuation and small size).

For most of these machines, rough-terrain performance and obstacle-crossing capabilities are not carefully documented in the literature. There are only a few examples in which such capabilities are reported in detail (Pugh et al. 1990; Bares and Wettergreen 1999), but even these are not suitable for assessing relative performance due to differences in scale and the lack of a consistent set of experiments and measures. Without more or less uniform standards of reporting, it becomes very difficult to test the claim that the relative speed (we use body lengths per second), relative endurance (we use specific resistance but also provide actual runtime data), and relative mobility (we provide a metric characterization of the various terrain features) of one design are superior to another. Thus, beyond the specifics of design and performance, we believe that the paper makes a distinct contribution to the robotics literature by establishing new standards of rigor in empirical performance reporting for legged vehicles.

In summary, we believe this new design opens up a large range of new possibilities for control of locomotion while still

meeting the constraints imposed by contemporary actuation and energy storage technology on engineering autonomous robotic platforms. At the present time, we are unable to provide a mathematically informed analysis of how and why RHex performs over the range of reported behaviors. Instead, in this first archival paper, we present careful empirical documentation of a narrow but very useful behavioral suite—a base range of locomotion capabilities at relatively high speeds over relatively challenging terrain—and observe that no other power autonomous legged design has ever before been demonstrated to exhibit a comparable breadth of mobility behaviors.

2. Design and Modeling

2.1. Design Concept and Morphology

In all robotics applications, mechanical complexity is one of the major sources of failure and considerably increases the cost. Our design emphasizes mechanical simplicity and thereby promotes robustness. Autonomy, a critical component of our aspiration toward real-world tasks in unstructured environments outside the laboratory, imposes very strict design constraints on the hardware and software components. Autonomy is often impossible to achieve with simple modifications to a system otherwise designed for nonautonomous operation. These constraints also justify our preference for overall simplicity—in particular toward minimizing the amount of actuation and limited reliance on sensing.

Our design, depicted in Figure 3, consists of a rigid body with six compliant legs, each possessing only one independently actuated revolute degree of freedom. The attachment points of the legs as well as the joint orientations are all fixed relative to the body.
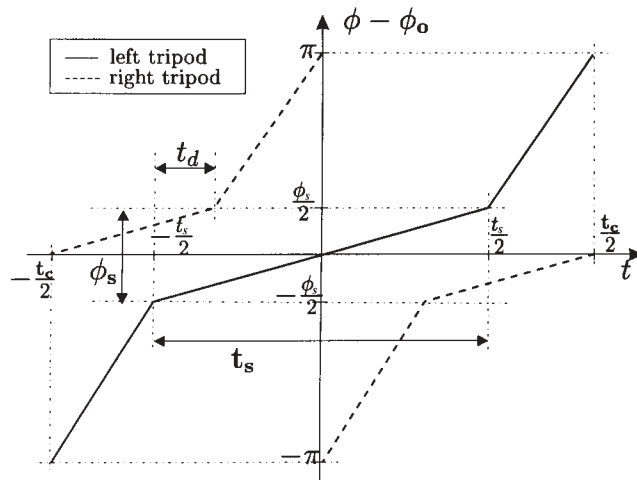

Fig. 4. Motion profiles for left and right tripods.

This configuration admits an alternating tripod gait for forward and backward locomotion, and possibly other more elaborate behaviors such as leaping, stair climbing, and so on. Moreover, the symmetry of this idealized model allows identical upside-down operation and imposes no restrictions on forward directionality. We explore some of this behavioral repertoire both in simulation and experimentally in Section 4 and Section 5, respectively.

2.2. Compliant Hexapod Model

In this section, we present a dynamical model of the morphology described in the previous section. Prior to the construction of the experimental prototype, this model enabled us to assess the viability of the design through simulation studies. Augmented with the actuator model of Section 4.1, it proved to be an invaluable tool in the design process.

Two reference frames, $\mathcal{B}$ and $\mathcal{W}$, are defined in Figure 3, the former attached to the hexapod body and the latter an inertial frame where the dynamics are formulated. In $\mathcal{B}$, we define the $+y$-direction to be *forward* and the $+x$-direction to be the *right side* of the robot. The position and orientation of the rigid body are described by $\mathbf{r_b} \in \mathbb{R}^3$ and $\mathbf{R_b} \in SO(3)$, respectively, expressed in $\mathcal{W}$. Table 2 details the notation used throughout the paper.

Each leg is assumed to be massless and has three degrees of freedom. The leg state is described in spherical coordinates $[\theta_i, \phi_i, \rho_i]^T$ whose origin is at $\mathbf{a_i}$ in the body frame.[5]

2.3. Equations of Motion

Our formulation of the equations of motion for the hexapod model is based on individually incorporating the ground reaction forces at each leg. To this end, it will suffice to analyze a generic leg parameterized by its attachment and touchdown points, $\mathbf{a_i}$ and $\mathbf{f_i}$, respectively. As a consequence of the assumption that the leg is massless, the rigid body experiences the ground reaction force on the leg, resulting in effective force and torque vectors acting on the center of mass. For each leg $i = 1, ..., 6$, following projections on $\mathcal{B}$, we have

$$\mathbf{F_i} = \begin{bmatrix} -\cos\theta_i \sin\phi_i & \sin\theta_i \sin\phi_i & -\cos\phi_i \\ \sin\theta_i & \cos\theta_i & 0 \\ \cos\theta_i \cos\phi_i & -\sin\theta_i \cos\phi_i & -\sin\phi_i \end{bmatrix}.$$
$$\begin{bmatrix} F_{r_i} \\ \tau_{\theta_i}/\rho_i \\ \tau_{\phi_i}/(\rho_i \cos\theta_i) \end{bmatrix}$$
$$\tau_i = (\bar{\mathbf{v}}_i + \mathbf{a_i}) \times \mathbf{F_i} ,$$

which are the force and torque contributions of a single leg to the overall system dynamics, respectively. The cumulative

---

5. Note that $(\mathbf{r_b}, \mathbf{R_b})$, $\mathbf{v_i}$ and $\mathbf{f_i}$ are related through the coordinate transformation $-\mathbf{R_b}(\mathbf{a_i} + \bar{\mathbf{v}}_i) = \mathbf{f_i} + \mathbf{r_b}$.

Table 2. Notation

States	
$\mathbf{r_b}, \mathbf{R_b}$	Body position and orientation
α	Body yaw angle
Leg states and parameters	
$\mathbf{a_i}$	Leg attachment point in $\mathcal{B}$
$\mathbf{f_i}$	Toe position in $\mathcal{W}$
$\mathbf{v_i}$	$:= [\theta_i, \phi_i, \rho_i]^T$ leg state in spherical coordinates
$\mathbf{\bar{v}_i}$	$:= [v_{x_i}, v_{y_i}, v_{z_i}]^T$ leg state in Cartesian coordinates
leg_i	Stance flag for leg i
Forces and torques	
F_{r_i}	Radial leg spring force
τ_{θ_i}	Bend torque in θ_i-direction
τ_{ϕ_i}	Hip torque in ϕ_i-direction
Controller parameters	
t_c	Period of rotation for a single leg
t_s	Duration of slow leg swing
ϕ_s	Leg sweep angle for slow leg swing
ϕ_o	Leg angle offset
$\mathbf{u}$	$:= [t_c, t_s, \phi_s, \phi_o]$ control vector
$\Delta\phi_o$	Differential change in ϕ_o for turning
Δt_s	Differential change in t_s for turning

effect of all the legs on the body is simply the sum of the individual contributions from the legs in contact with the ground, together with the gravitational force:

$$\mathbf{F_T} = \begin{bmatrix} 0 & 0 & -mg \end{bmatrix}^T + \mathbf{R_b} \sum_{i=1}^{6} leg_i \mathbf{F_i} \qquad (1)$$

$$\tau_T = \mathbf{R_b} \sum_{i=1}^{6} leg_i \tau_i . \qquad (2)$$

The contact states of the legs are indicated by leg_i. In consequence, the dynamics of the hexapod are governed by the standard rigid-body dynamics under external torque and force inputs (Goldstein 1980). Note also that the discrete transitions in the contact states of the legs result in a hybrid dynamical system whose behavior can be substantially different than that of its continuous constituents alone.

3. Control Strategy

The present prototype robot has no external sensors by which its body state may be estimated. Thus, in our simulations and experiments, we have used joint space closed-loop ("proprioceptive") but task space open- loop control strategies. The algorithms that we describe in this section are tailored to demonstrate the intrinsic reliability of the compliant hexapod morphology and emphasize its ability to operate without

a sensor-rich environment. Specifically, we present a four-parameter family of controllers that yields translation and turning of the hexapod on flat terrain without explicit enforcement of quasi-static stability. In Section 5.3, we demonstrate the capabilities of this family of controllers on our experimental platform over a wide range of terrain conditions, from flat terrain to a rough, broken surface.

All controllers generate periodic desired trajectories for each hip joint, which are then enforced by six local PD controllers (one for each individual hip actuator). In this respect, the present controller family represents one near-extreme along the spectrum of possible control strategies, ranging from purely feedforward (i.e., taking no notice of body state) to purely feedback (i.e., producing torque solely in reaction to leg and rigid-body state). It seems likely that neither of these extremes is best and a combination should be adopted. The simulations and experiments presented in this paper attempt to characterize the properties associated with the sensorless feedforward extreme, which, when RHex has been endowed with sensors, we hope to complement with feedback to explore the aforementioned range.

An alternating tripod pattern governs both the translation and turning controllers, whereby the legs forming the left and right tripods are synchronized with each other and are 180 degrees out of phase with the opposite tripod, as shown in Figure 4.

3.1. Forward Alternating Tripod Gait

The open-loop controller's target trajectories for each tripod are periodic functions of time, parameterized by four variables: t_c, t_s, ϕ_s, and ϕ_o. In a single cycle, both tripods go through slow and fast swing phases, covering ϕ_s and $2\pi - \phi_s$ of the complete rotation, respectively. The period of both profiles is t_c. In conjunction with t_s, it determines the duty factor of each tripod with respect to the duration of its slow and fast phases. The time of "double support" t_d (where all six legs are in their slow phases but possibly not all of them are touching the ground) is hence determined by the duty factors of both tripods. Finally, the ϕ_o parameter offsets the motion profile with respect to the vertical (see Fig. 4). Note that both profiles are illustrated to be monotonically increasing in time, but they can be negated to obtain backward locomotion.

Control of locomotion is achieved by modifying these parameters for a particular desired behavior during locomotion. In Section 4, our simulation studies reveal correlations of these parameters with certain behavioral attributes.

3.2. Turning

We developed two different controllers for two qualitatively different turning modes: turning in place and turning during translation. These controllers are inspired by differential

turning in wheeled and tracked vehicles, where opposite perturbations to contralateral actuators result in a net rotation of the body on the plane. Analytical understanding of this behavior in the context of our design awaits careful mathematical treatment of RHex's dynamics as well as accurate models of ground contact.

The controller for turning in place employs the same leg profiles as for forward locomotion except that contralateral sets of legs rotate in opposite directions. This results in the hexapod turning in place in the direction determined by the rotational polarity of the left and right sets of legs. Note that the tripods are still synchronized internally, maintaining three supporting legs on the ground. Similar to the control of the forward locomotion speed, the rate of turning depends on the choice of the particular motion parameters, mainly t_c and ϕ_s.

In contrast, we achieve turning during forward locomotion by introducing differential perturbations to the forward-running controller parameters for contralateral legs. In this scheme, t_c is still constrained to be identical for all legs, which admits differentials in the remaining profile parameters, ϕ_o and t_s, while ϕ_s remains unchanged. Two new gain parameters, Δt_s and $\Delta\phi_o$, are introduced. Turning right (toward $+x$ in the coordinate system of Fig. 3, defining $+y$ as forward) is achieved using $\mathbf{u}_l = [t_c, t_s + \Delta t_s, \phi_s, \phi_o + \Delta\phi_o]$ and $\mathbf{u}_r = [t_c, t_s - \Delta t_s, \phi_s, \phi_o - \Delta\phi_o]$ for the legs on the left and right sides, respectively.

4. Simulation Studies

Our simulation studies in this section use the dynamical model described in Section 2.2 together with an actuator model to demonstrate the feasibility of basic locomotion behaviors of our design under practical actuation limitations. The presented results provide a proof of concept for the design, justifying the building of our prototype and the extensive experiments of later sections. To limit the scope of the paper to an appropriate length, however, we have excluded impact of these models and the resulting simulation tools in refining the kinematic and dynamical parameters of our experimental prototype.

4.1. Actuator Model

The model of Section 2.2 does not impose any constraints on the choice of the hip torques τ_{ϕ_i}. In practice, however, torque limitations are one of the major challenges in the design of autonomous legged vehicles, even for statically stable modes of operation. To capture this aspect of our design space in the subsequent simulation studies, we incorporate a simple model of the hip actuation.

Figure 5 portrays the torque-speed characteristics for the DC motors used in our experimental platform. The shaded band captures the range of torque deliverable by the motor
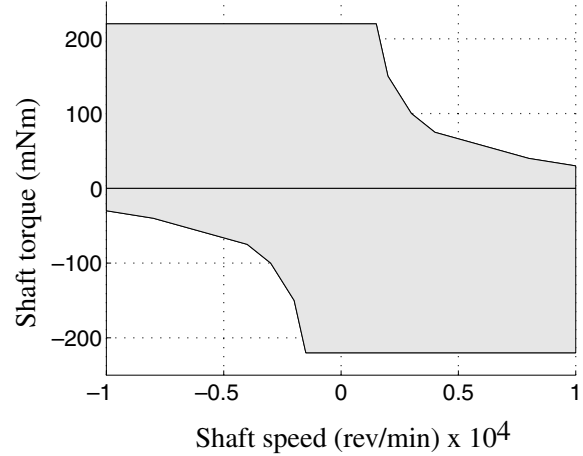

Fig. 5. Torque characteristics for the Maxon RE118751 20-W DC motor, reproduced from the manufacturer's datasheet. The shaded band illustrates the range of torque deliverable by the motor.

at any particular speed.[6] Our simulations incorporate this model by saturating hip torque command outputs of the local PD controllers as a function of the leg angular velocity.

4.2. Simulation Environment

All the simulation results of the next section were produced by SimSect, a simulation environment that we created primarily for the study of the compliant hexapod platform (Saranli 2000). SimSect can efficiently and accurately deal with the hybrid nature of our model resulting from its discrete ground contact states, still preserving the relatively simple dynamics of the continuous model.

The hexapod simulation with SimSect uses the same dimensions and body mass as our experimental platform (see Section 5). However, some of the dynamical parameters used in the simulations, including the leg spring and damping constants, and the ground friction coefficient are not experimentally verified and are likely to be different from their actual values. Nevertheless, the relatively accurate match between the simulations and the experimental platform with regard to their morphology and mass parameters still admit qualitative comparisons of behavior.

4.3. Simulation Results

In this section, we verify in simulation that the controllers of Section 3 are able to produce fast, autonomous forward locomotion of the hexapod platform.

Figure 6 shows the forward velocity (a) and the turning yaw rate (b) as functions of controller parameters t_c and ϕ_s.

---

6. Note that the we have conservatively approximated the DC motor characteristics by assuming constant maximum torque for second and fourth quadrants.

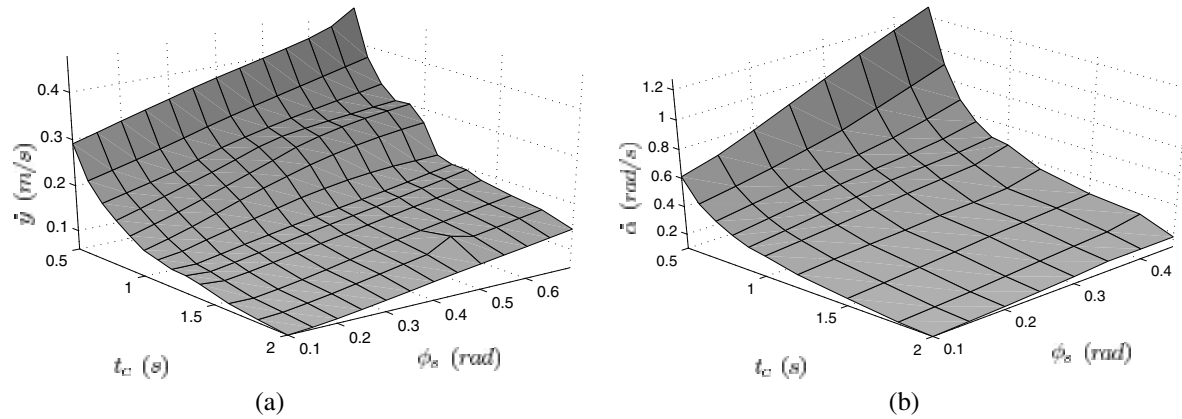(a)   (b)

Fig. 6. (a) Average forward velocity $\dot{y}$ as a function of t_c and ϕ_s over 5 seconds of operation, during which the robot always settled down to an approximately periodic trajectory. Remaining controller parameters are chosen as $t_s = t_c/2$, $\phi_o = 0$. (b) Average in-place turning yaw rate $\dot{\alpha}$ as a function of t_c and ϕ_s over 5 seconds of operation.

Although the remaining parameters t_s and ϕ_o have a considerable effect on the body oscillations during locomotion and the forward velocity, through manual tuning we identified certain values for them to yield good performance in most cases. As a consequence, throughout these simulations, ϕ_o is kept constant and t_s is chosen to be half the stance time. Nevertheless, it is clear that proper tuning of all four controller parameters is necessary to achieve the smoothest and fastest locomotion performance. The effects of a hand-tuned, intuitively "best" choice for a given t_c and ϕ_s is demonstrated in Figure 7 and the associated Extension 5, a typical forward translation with an average velocity of 0.55 m/s.

These results suggest the opportunities for considerably improved performance resulting from the introduction of feedback to regulate the forward locomotion and turning yaw rate of the compliant hexapod platform. We sketch our approach to these future opportunities in the conclusion.

5. Experimental Platform

5.1. Hardware Description

We built an experimental platform (Fig. 1) as an instantiation of the design concepts of Section 2.1. RHex is an autonomous hexapod robot with compliant legs, very close to the model described in Section 2.2. All the computational and motor control hardware is on board, together with two Panasonic 12-V, 2.2-Ah sealed lead-acid batteries for power autonomous operation. A PC104 stack with a 100-MHz Intel 486 microprocessor, together with several I/O boards, performs all the necessary computation and implements the controllers of Section 3. A remote control unit provides the user input for giving higher level commands such as the forward speed and turning direction, presently via a joystick.

Each leg is directly actuated by a Maxon RE118751 20-W brushed DC motor combined with a Maxon 114473 two-stage

33:1 planetary gear (Interelectric AG, Sachseln, Switzerland), delivering an intermittent stall torque of 6 Nm. The motor angle and, thus, the leg angles are controlled via 1-kHz software PD control loops. The control software also features several safety measures, including fault detection for the encoders, estimation of the rotor temperatures to avoid motor damage, and a watchdog timer that disables the motors and resets the computer in case of software failure.

The main body measures $53 \times 20 \times 15$ cm and roughly matches the symmetries of the ideal model except for the slightly lower center of mass and the larger length of the bottom side. The legs are made from 1 cm diameter Delrin rods and are C-shaped to increase compliance in the radial direction and permit easy clamping to the gear shaft (see Extension 6). The leg length is 17.5 cm, measured as the vertical distance from ground to the gear shaft when standing up. We experimentally measured the radial compliance of these legs to be approximately 4500 N/m in their expected operating region. The encoder/motor/gear stacks protrude from the main body, and the maximum widths of the front and back legs amount to 39.4 cm, measured at half the leg length. To provide clearance for the rotating front and back legs, the motors for the middle legs are further offset and result in a maximum width of 52 cm. The total mass of the robot is 7 kg, with each leg contributing only approximately 10 g.

5.2. Visual Measurement Apparatus

Absent any inertial sensing on RHex, we devised a simple visual tracking system to record the robot's position and orientation in the sagittal (obstacle-crossing experiments) and the horizontal (turning and rough-surface experiment) planes. Four light-emitting diodes (LEDs) were attached to the robot's body, and a set of stationary calibration LEDs were placed close to the extremes of the camera's field of view. The experiments were then conducted in complete darkness, which
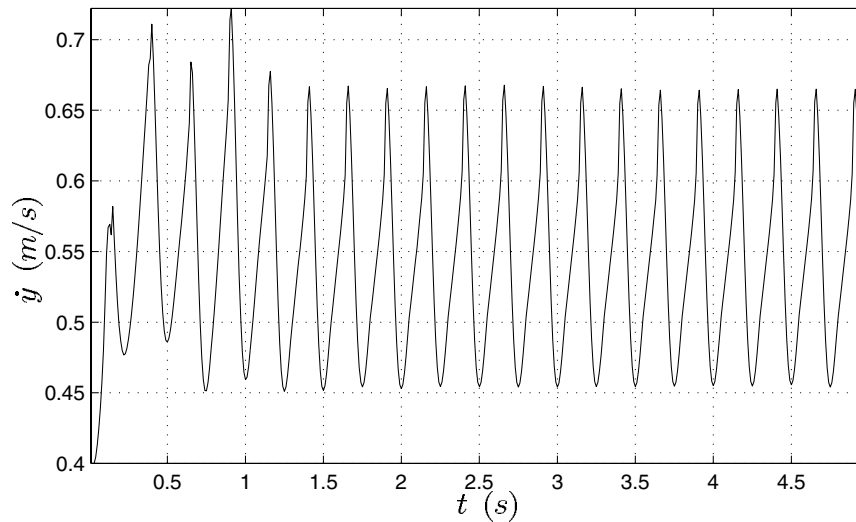
Fig. 7. Forward body velocity for a simulation run with $t_c = 0.5$ s, $\phi_s = 0.7$ rad, $t_s = 0.3$ s, and $\phi_o = 0.03$ rad.

allowed for very high contrast recordings of the LED markers. Because of this greatly simplified visual data, standard computer vision algorithms were then employed to extract the planar robot position and orientation with up to 1% accuracy in the average velocity computations.

5.3. Experimental Results

In the sequel, we will document the robot's speed over various terrains, maneuverability, obstacle-crossing capability, and payload. Furthermore, energy efficiency and runtime are critical performance criteria for any untethered robot. Thus, the energetic performance of the robot is carefully documented, but it must be noted that at the time of this writing, no efforts have been made to optimize it. All experiments—except the random obstacles experiment—were run untethered, and we document the average power consumption based on recordings of the battery voltage and current.

To measure energy efficiency, we use the "specific resistance" (Gabrielli and von Karman 1950), $\varepsilon = P/(mgv)$, based on the robot's weight, mg, and its average power consumption, P, at a particular speed, v. Specific resistance was originally used to compare the energy efficiency of animals of vastly different sizes, where the average power measured the rate of metabolic energy expenditure based on oxygen consumption. The same measure has been used to compare the energy efficiency of a range of different robots (Ahmadi and Buehler 1999; Gregorio, Ahmadi, and Buehler 1997; Hirose 1984; Waldron and Vohnout 1984). Unfortunately, attention to energy efficiency and its reporting is fairly rare in robotics and is not consistent. For example, the power, if documented at all, is given as the mechanical power delivered by the actuators, the peak mechanical power of the main power

source, or the total electrical power consumption. Therefore, quantitative energetic comparisons of past robots are not always precise. For electrically actuated mobile robots such as RHex, it makes most sense to report the total electrical power consumption (which includes the power for sensing and computing) because it will determine, together with the battery capacity, the all-important runtime. In any case, the battery power consumed will always provide an upper bound on joint power or mechanical power because the battery is the only source of energy in the system.

Throughout the experiments, the control parameters were set to fixed values, and these values were only modified by the operator via the joystick commands in an attempt to steer the robot along a straight line. The speed command input was used solely for starting and stopping the robot.

Experimental findings are summarized in Table 3 and Figures 8 and 9. A detailed account of the setup, measurement protocols, and failure modes is presented in Appendix B.

5.3.1. Forward Locomotion

This first set of experiments documents RHex's maximum velocity, power, and specific resistance with the two-stroke open-loop controller of Section 3 while traversing carpet (see Extension 7 for an example run), linoleum, grass, and coarse gravel. The robot moved well over these indoor and outdoor surfaces, with only minor velocity variations between 0.45 m/s and 0.55 m/s, as shown in Figure 8. The velocity on linoleum was lowest due to intermittent slipping, which also causes a larger standard deviation of the runs compared to carpet. In the current prototype, the relatively high natural frequency of the system and the open-loop nature of the leg trajectories limit the maximum speed due to

Table 3. Experimental Statistics

	Carpet	Linoleum	Grass	Gravel	Rough	Single Obstacle	Comp. Const.	Obstacle Course
Total number of runs	10	11	16	25	32	14	14	26
Successful runs	10	10	10	10	16	10	10	10
Electronics and hardware problems	—	—	1	5	6	—	—	2
Deviation from course	—	1	—	5	7	—	—	5
Operator mistake[a]	—	—	5	5	—	3	2	2
Stuck on obstacle	—	—	—	—	3	1	2	7

[a]These failure modes include steering in unwanted directions, failure to trigger the timing switch, and the power cord wrapping around the legs.
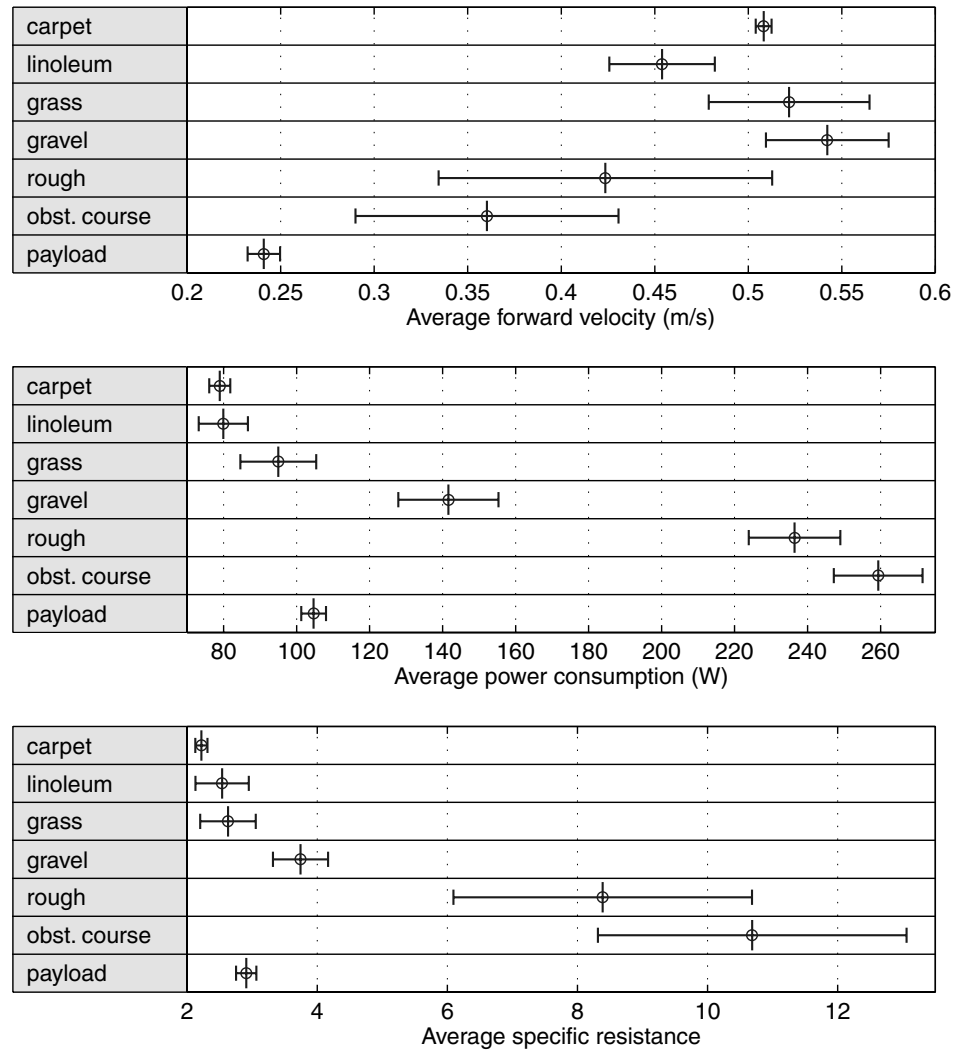

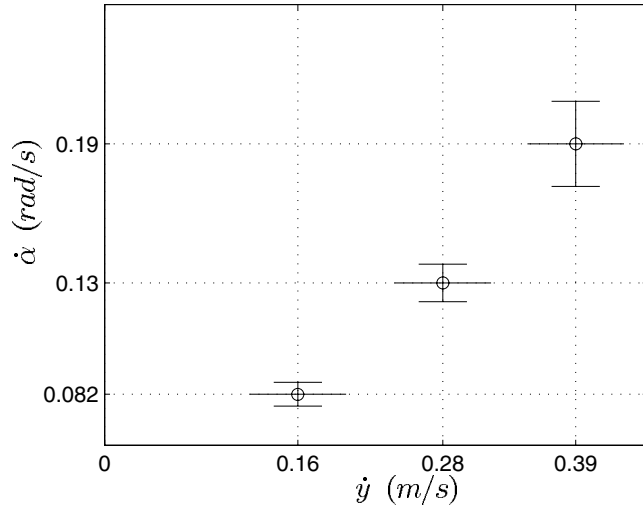Fig. 8. Comparison of average forward velocity and energetics for different experiments (see also Extension 8).

Fig. 9. Turning yaw rate as a function of forward velocity. See Extension 9 for all the data and analysis scripts associated with the turning experiments.

out-of-phase vertical body oscillations, which reduce traction. The surface irregularities of the outdoor grass and gravel surfaces provided improved traction and, therefore, average velocities slightly above 0.5 m/s, but they also resulted in larger variations between the runs. The specific resistance (power consumption) was lowest on carpet with 2.21 (80 W) and highest on gravel with 3.74 (140 W). We experimented with control parameter settings to reach the maximum robot velocity on office carpet and linoleum and selected $\mathbf{u} = [0.45, 0.2, 51, 0]$. The grass and gravel surfaces were not tested with these settings prior to the reported experiments. Figure 8 shows the average velocity, power consumption, and specific resistance over 10 runs, with standard deviations for all the experiments. All the experimental data as well as the associated analysis scripts can be found in Extension 8. Table 3 summarizes the failure modes and statistics for all the experiments described in this section.

5.3.2. Turning

As our simulation study predicted, steering is possible, even though the leg actuation is limited to motion in the sagittal plane only via differential motion between left and right legs. We selected control parameters that resulted in turns in place and robot speeds up to about 0.4 m/s (see Table 4) on most flat surfaces including carpet, linoleum, grass, and gravel. The maximum forward velocity is reduced during turning because the differential leg motion precipitates the onset of the speed-limiting vertical body oscillations. The maximum yaw angular velocities increase almost linearly with forward velocity up to 0.19 rad/s at 0.39 m/s, as illustrated in Figure 9.

Interestingly, the resulting turn radius remains roughly constant at 2 m for different settings of the forward velocity. Turning in place provides the highest yaw angular velocity of 0.7 rad/s, although it is not possible to directly compare its performance to differential turning, which is a qualitatively different controller. At present, we do not understand completely the relationship between the controller parameters and effective yaw rates, a subject of ongoing research.

5.3.3. Obstacle Crossing

The obstacle-crossing capabilities of the simple open-loop walking controller were evaluated with two different obstacles—a 15 cm high Styrofoam block and a composite obstacle with a maximum height of 22 cm, as shown in Figures 10 and 11, respectively (see also Extensions 10 and 11). The robot was able to surmount both obstacles, neither sensing them nor with any modification to the control parameters of the walking experiments. The data in the top portions of the two graphs show the forward velocity averages (over 10 runs) before, during, and after the obstacle. Surprisingly, the average velocity decreases only slightly as the robot climbs over the obstacle and increases again afterward. Because the robot's trajectory over the obstacle depends greatly on how the legs engage it, the standard deviation of the average velocities increases over the obstacle. The average speed varied most (with the largest standard deviation) following the end of the composite obstacle because the robot's recovery speed depended on how the robot landed on the ground. As a further illustration of the robot's motion, the forward velocity from a particular run and the robot's body in the sagittal plane at 0.5-second intervals during the same run are shown.

5.3.4. Obstacle Course

To demonstrate RHex's rough-terrain capabilities, we constructed the obstacle course depicted in Figure 12. It consisted of 10 randomly spaced obstacles of 12.2 cm height (i.e., 60% of the leg length and exceeding ground clearance by 1.8 cm). This was by far the most challenging of the experiments, requiring the largest number of runs before 10 successful completions. Most failures can be attributed to the open-loop nature of the walking controller, which had to climb blindly over 10 randomly spaced obstacles, sometimes as little as half a body width apart, but all higher than the ground clearance. This had to be done successfully over a distance of 8.13 m, avoiding all the failure modes detailed in Appendix B. Yet, for the 10 successful runs, RHex was able to maintain an average velocity of 0.36 m/s over the length of the obstacle course (Fig. 8). The best run finished in only 17.78 seconds, or an average velocity of 0.46 m/s, with a specific resistance of 8.17. The punishing nature of this course is reflected in the power consumption of more than three times that of walking on carpet, more than five times the specific

Table 4. Controller Parameters for Turning at Different Speeds

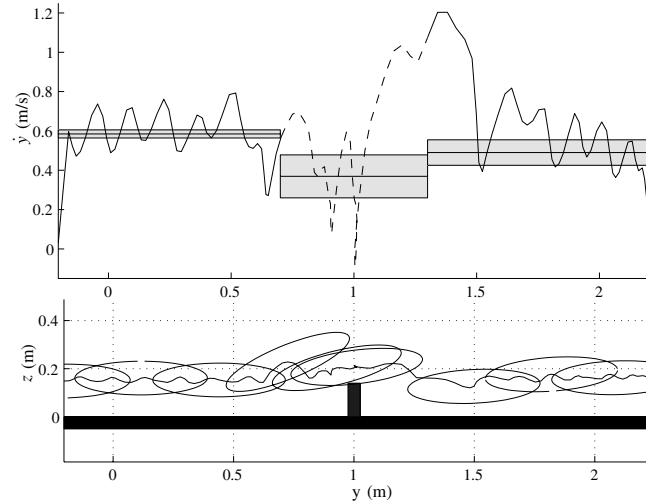| $\dot{x}$ (m/s)	t_c (s)	t_s (s)	ϕ_s (rad)	ϕ_o (rad)	$\Delta\phi_o$ (rad)	Δt_s (s)
0	1.0	0.6	35	0.0	0.0	0.0
0.16	1.2	0.7	25	0.0	6.0	−0.02
0.28	0.8	0.45	35	0.0	7.5	0.0
0.39	0.53	0.33	40	0.0	6.5	0.0

Fig. 10. Sagittal plane data during simple obstacle crossing. The data in the top portion of the graph show forward velocity averages and standard deviations (over 10 runs) before, during, and after the obstacle. The solid and dashed line is one particular run. The bottom half shows a projection of the robot's body onto the sagittal plane in 0.5-second intervals (horizontal and vertical axes at the same scale). See Extension 12 for all the experimental data and analysis scripts.

resistance, and a high rate of component breakdown: during the obstacle course experiments, RHex broke three legs, burned several circuit traces, and fractured its frame.

5.3.5. Rough Surface

This last rough terrain experiment is an attempt to evaluate RHex's performance in an environment similar to that negotiated by the Blaberus cockroach in Full et al. (1998). Our efforts at recreating such a surface at RHex's scale can be evaluated visually in Figure 2 as well as Extensions 3 and 4. To our surprise, RHex was able to traverse this surface with random height variations of up to 20.32 cm (116% leg length) (Fig. 13) with relative ease at an average velocity of 0.42 m/s (Fig. 8). RHex's planar trajectories during the two fastest and the two slowest successful runs are shown in Figure 14. In addition, body state associated with all the rough surface runs can also be found in Extension 14.
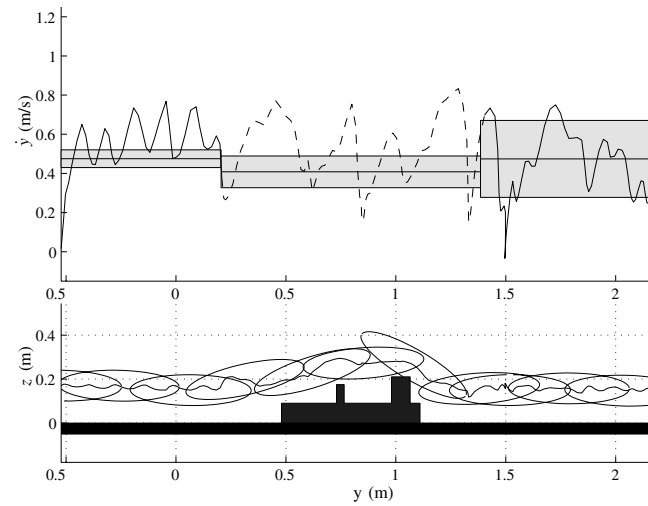

Fig. 11. Sagittal plane data during composite obstacle crossing. The data in the top portion of the graph show forward velocity averages and standard deviations (over 10 runs) before, during, and after the obstacle. The solid and dashed line is one particular run. The bottom half shows a projection of the robot's body onto the sagittal plane in 0.5-second intervals (horizontal and vertical axes at the same scale). See Extension 13 for all the experimental data and analysis scripts.
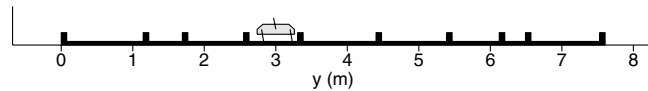

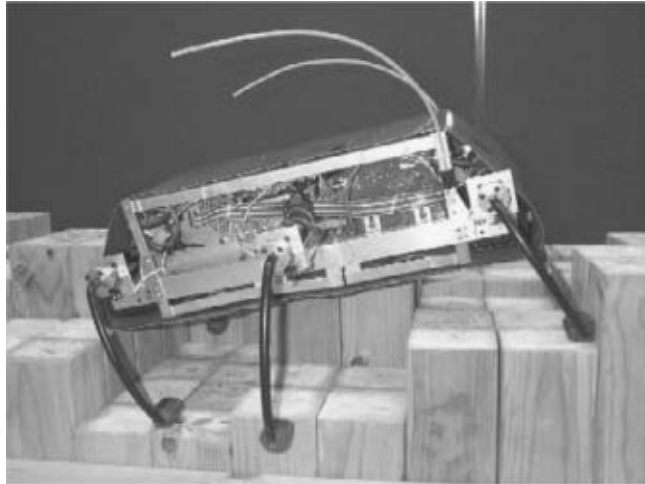
Fig. 12. Scale drawing of RHex and the obstacle course.

Fig. 13. Sample profiles of row 6 (columns 8, 9, and 10) with RHex statically posed for comparison.

5.3.6. Payload and Runtime

To demonstrate RHex's payload capacity, we mounted an additional mass of 7.94 kg (one 10-lb and one 7.5-lb weight-lifting barbell) to the bottom of RHex's body and adjusted the control parameters for lower speed and a small sweep angle ($c_6 = 0.7, 0.2, 14, 0$). The robot was able to transport this additional mass, more than its own total mass, at about half its maximum speed (0.25 m/s) with a specific resistance of about 3. These averages were obtained from 10 runs. This payload is close to the limit of the current design and may not be practical, since the motors are not powerful enough to raise the robot when lying on the floor even when all six legs are used. A careful analysis of trade-offs between payload and speed in legged systems operating in a quasi-static regime is provided in Huang and Waldron (1990) but is not directly applicable to RHex.

Finally, the endurance of RHex was tested in standby mode (with the motors enabled and maintaining a standing position) and while walking at maximum speed on carpet. The average runtime was 48 minutes for standby and 18 minutes for uninterrupted walking, both values averaged over five experiments in each setting.

6. Conclusion

Nimble, robust locomotion over general terrain remains the sole province of animals, notwithstanding our functional prototype, RHex, or the generally increased recent interest in legged robots. RHex, endowed with only a rudimentary controller, uses what might be termed the engineering equivalent of preflexes (Brown and Loeb 2000; Full et al. 1998) to negotiate relatively badly broken terrain at relatively high speeds—performance beyond that heretofore reported for autonomous legged vehicles in the archival literature. We are convinced

that further systematic application of certain operational principles exhibited by animals will achieve significant increases in RHex performance and inform the evolution of the underlying mechanical design of future prototypes. To conclude the paper, we provide a brief sketch of these principles and how they may be applied.

Accumulating evidence in the biomechanics literature suggests that agile locomotion is organized in nature by recourse to a controlled bouncing gait wherein the "payload," the mass center, behaves mechanically as though it were riding on a pogo stick (Blickhan and Full 1993). While Raibert's (1986) running machines were literally embodied pogo sticks, more utilitarian robotic devices such as RHex must actively anchor such templates within their alien morphology if the animals' capabilities are ever to be successfully engineered (Full and Koditschek 1999). We have previously shown how to anchor a pogo stick template in the more related morphology of a four-degree-of-freedom monopod (Saranli, Schwind, and Koditschek 1998). The extension of this technique to the far more distant hexapod morphology surely begins with the adoption of an alternating tripod gait, but its exact details remain an open question, and the "minimalist" RHex design (only six actuators for a six-degree-of-freedom payload) will likely entail additional compromises in its implementation. Moreover, the only well-understood pogo stick is the spring-loaded inverted pendulum (Schwind and Koditschek 2000), a two-degree-of-freedom sagittal plane template that ignores body attitude and all lateral degrees of freedom. Recent evidence of a horizontal pogo stick in sprawled-posture animal running (Kubow and Full 1999) and subsequent analysis of a proposed lateral leg spring template to represent it (Schmitt and Holmes 2000) advance the prospects for developing a spatial pogo stick template in the near future. Much more effort remains before a functionally biomimetic six-degree-of-freedom payload controller is available, but we believe that the present understanding of the sagittal plane can already be used to significantly increase RHex's forward speed and endow our present prototype with an aerial phase.

Appendix A: Details of the Experimental Setup and Failure Modes

Forward Locomotion

We ran the robot over carpet, linoleum, grass, and gravel. The carpet and linoleum surfaces were standard office floors found close to the lab. The grass was wet on the day of the experiment and showed height variations of about 2 cm. The gravel patch contained fairly large gravel pieces (see Fig. 1) between 3 and 8 cm diameter. For all the experiments, the robot was driven over a test stretch of 2 m. To obtain precise timing and to synchronize the data logging with the test stretch, a switch was mounted in the front of the robot, which was triggered as the robot ran into a Styrofoam panel held at the beginning
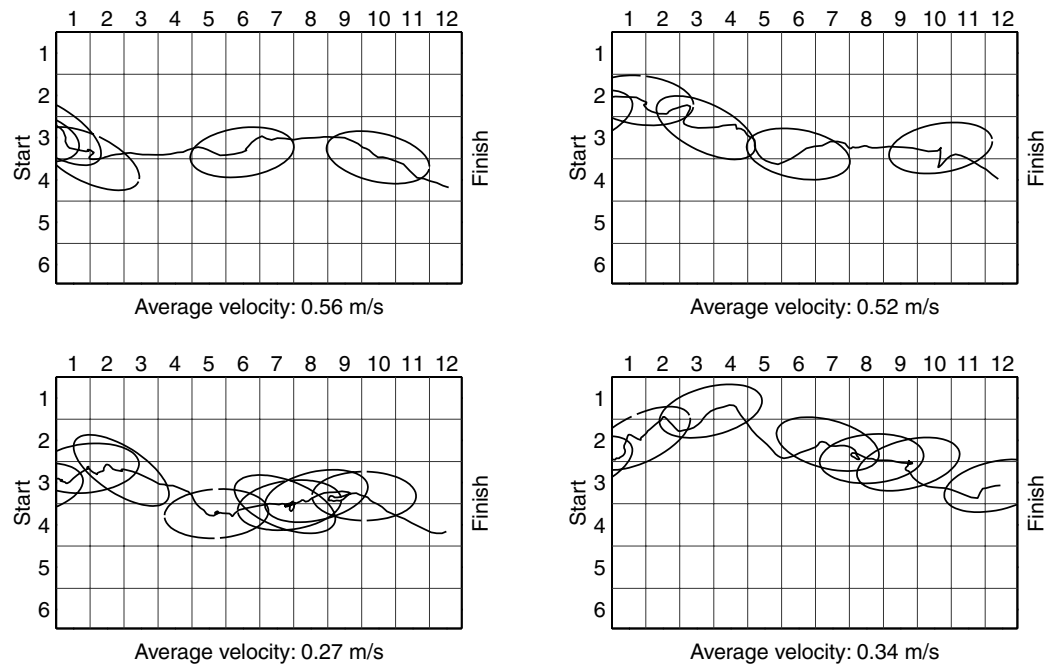
Fig. 14. The two fastest (top) and the two slowest (bottom) robot trajectories in the horizontal plane as RHex moves over the rough surface. The plots also show projections of the body onto the horizontal plane in 1-second intervals. See Extension 14 for all the experimental data and associated analysis scripts.

and the end of the test stretch. The runs over each surface were repeated until 10 successful runs were obtained. The average velocity and power consumption for each run were then computed with the available data.

Ten successive experiments were run for the carpet surfaces with no failures. One run on the Linoleum floor was discarded because the robot deviated too much from the straight line. A total of 16 runs on grass were necessary, with 6 runs discarded. In 5 runs, the operator failed to align the start or stop trigger panel properly, and the front legs pushed it aside, preventing the switch to be actuated. One run was abandoned due to remote control noise in the remote control command input. Gravel was more challenging; of the 25 runs, 5 were discarded because the robot deviated too much from a straight line, 5 were discarded because of the operator missing the trigger switch, 1 was discarded because of remote control noise, and 4 were discarded because the front switch broke on impact with the trigger panel.

Turning

The turning experiments were run on carpet. To reduce the data processing for this set of experiments, only 6 runs were processed in this fashion for each forward velocity instead of the usual 10. Only a few runs were discarded because of noise in the remote control, which interfered with the velocity and/or the steering command.

Obstacle Crossing

The first obstacle was a 1.22 m long strip of 3 in. (7.62 cm) thick Styrofoam board, a standard insulating construction material, cut to 15 cm height. This represents 80% of the robot's leg length and exceeds its 10.5-cm ground clearance by 4.6 cm, or almost 50%. The Styrofoam was chosen for this experiment, as well as the random obstacle course described below, for its ready availability, low cost, and ease of cutting. It is softer than wood yet hard enough that the robot does not deform it. The second obstacle was built from construction lumber and consisted of a 10 cm high and 63 cm wide base (as viewed in the sagittal plane) on top of which an 8.5 cm high and 3.5 cm wide block was mounted at a distance of 25 cm from the front and a 12.5 cm high and 8.5 cm wide second block was mounted at a distance of 50 cm from the front. In both experiments, the control parameters were the same as in the walking experiments above. All data shown were obtained by the visual tracking procedure described in Section 5.2, with the camera oriented for a perpendicular view of the sagittal plane. The average forward velocity of each run was obtained before, over, and after the obstacle.

Fourteen successive experiments were required and logged for both obstacles. From the runs over the first obstacle, the robot failed to surmount it only once, but the vision postprocessing algorithm failed to extract reliable position data for 3 successful runs, when the robot's direction after obstacles deviated significantly from a straight path. From the 14

	1	2	3	4	5	6	7	8	9	10	11	12
1	12"	8"	4"	7"	11"	12"	9"	6"	6"	7"	7"	8"
2	9"	4"	11"	8"	8"	10"	11"	5"	12"	6"	9"	12"
3	9"	8"	10"	9"	6"	10"	8"	5"	4"	7"	5"	6"
4	10"	6"	12"	10"	9"	11"	8"	8"	9"	6"	5"	8"
5	5"	11"	10"	10"	10"	12"	5"	11"	8"	10"	6"	8"
6	4"	9"	7"	8"	10"	8"	5"	6"	9"	12"	9"	11"

(Start at left, Finish at right)

Fig. 15. Height distribution over the rough surface.

successive runs over the composite obstacle, the robot failed twice to surmount the obstacle, and the vision postprocessing failed to extract data from the postobstacle portion of 2 runs.

Obstacle Course

The experimental setup for the obstacle course consisted of 10 randomly spaced obstacles of 12.2 cm height. The free spaces between the ten 3 in. (7.62 cm) wide Styrofoam blocks were 1.07, 0.47, 0.78, 0.68, 1.02, 0.91, 0.66, 0.29, and 0.96 m, selected between 0.5 and 2 body lengths from a uniform random distribution. Thus, the total obstacle course extended over 8.13 m, which also includes one half body length before and after the course. The time between start and finish was measured via a stopwatch. During these experiments, an operator attempted to keep the robot on course using the limited directional control described above. Nevertheless, the directional disturbances due to the obstacles caused the robot at times to veer toward the lateral limits of the 1.2 m wide course. In those instances, operators who followed the robot along the course placed a Styrofoam panel along the lateral limits to make up for the lack of side walls. When the collision angle with these walls was sufficiently small, the robot realigned itself with the course.

Because of the large number of runs required for this experiment and the high power requirements, we made an exception and ran the robot from higher capacity external batteries via an umbilicus. This greatly reduced the experimental effort by eliminating the need to recharge and exchange the onboard batteries. However, no performance improvement resulted from this arrangement compared to running on freshly charged onboard batteries. The onboard batteries were kept in place to maintain the total robot mass.

A total of 26 successive experiments on the obstacle course were recorded. Of these, 16 were discarded for the following reasons: the robot turned itself sideways beyond quick recovery (2); shut itself off (1); required operator intervention

through the remote control unit, such as turning in place or short reversal of direction to complete the course (3); turned itself on its back either by climbing up against the side walls (1) or the obstacle (3); wrapped the power cord around its legs (1); ended up "sitting," aligned with and on top of an obstacle and unable to reach the ground (3); or had burned electrical circuits (1). The remaining 11 runs were used to calculate the velocity, power, and specific resistance data shown in Figure 8.

Rough Surface

To recreate Full et al.'s (1998) rough surface, we compared the height distribution of his environment (R. J. Full, personal communication, June 1998) to checkerboard arrays of randomly uniformly distributed block heights. When scaled to RHex's dimensions, we decided that a height variation of between 4 in. (10.16 cm) and 12 in. (30.48 cm), or 1.16 leg lengths, was a good match (Fig. 15). To simplify cutting by a local lumber yard, the block heights were discretized to 1-in. (2.54-cm) increments. The block width of 7 in. (17.78 cm) permitted the use of four pieces of standard 3.5×3.5 in. $(8.89 \times 8.89$ cm) cross section lumber per checkerboard block. The total surface consisted of 72 blocks (6 by 12), thus requiring 288 individually cut lumber sections. The robot was run in the direction of the 12-block length of the surface, with wall panels on each side. Its Cartesian position and orientation, projected onto the horizontal plane, were measured with the visual tracking setup described above in the steering experiment.

We carried out 32 experiments on this surface, with a success rate of 50%. During the unsuccessful runs, the robot either ran head-on into a side wall or ran into one of the isolated posts (typically the isolated high block with coordinates 2,9 in Fig. 15) (3), broke a leg (2), hit one of the walls (3), or had to back up and continue forward (4). Also, 4 of the experiments were not completed due to remote control failure. From the

16 experiments that were successfully recorded, we used 10 with the cleanest vision data to facilitate the postprocessing.

Acknowledgments

References

Ahmadi, M., and Buehler, M. 1999. The ARL monopod II running robot: Control and energetics. *IEEE International Conference on Robotics and Automation*, Detroit, MI, May, pp. 1689–1694.

Altendorfer, R., Saranli, U., Komsuoglu, H., Koditschek, D. E., Brown, H. B., Jr., Buehler, M., Moore, N., McMordie, D., and Full, R. 2001. Evidence for spring loaded inverted pendulum running in a hexapod robot. In *Experimental Robotics*, ed. Rus, D., and Singh, S., pp. 291–302, New York: Springer.

Angle, C. 1989. Genghis: A six-legged autonomous walking robot. Ph.D. thesis, Massachusetts Institute of Technology.

Angle, C. 1991. Design of an artificial creature. Ph.D. thesis, Massachusetts Institute of Technology.

Bares, J. E., and Wettergreen, D. S. 1999. Dante II: Technical description, results and lessons learned. *International Journal of Robotics Research* 18:1–29.

Binnard, M. 1995. Design of a small pneumatic walking robot. Ph.D. thesis, Massachusetts Institute of Technology.

Blickhan, R., and Full, R. J. 1993. Similarity in multilegged locomotion: bouncing like a monopode. *Journal of Comparative Physiology A* 173:509–517.

Brown, I. E., and Loeb, G. E. 2000. A reductionist approach to creating and using neuromusculoskeletal models. In *Biomechanics and Neural Control of Movement*, ed. J. Winters and P. Crago. New York: Springer-Verlag.

Buehler, M., Battaglia, R., Cocosco, A., Hawker, G., Sarkis, J., and Yamazaki, K. 1998. SCOUT: A simple quadruped that walks, climbs and runs. *IEEE International Conference on Robotics and Automation*, Leuven, Belgium, May, pp. 1707–1712.

Buehler, M., Cocosco, A., Yamazaki, K., and Battaglia, R. 1999. Stable open loop walking in quadruped robots with stick legs. *IEEE International Conference on Robotics and Automation*, Detroit, MI, May, pp. 2348–2353.

Chiel, H. J., Beer, R. D., Quinn, R. D., and Espenschied, K. S. 1992. Robustness of a distributed neural network controller for locomotion in a hexapod robot. *IEEE Transactions on Robotics and Automation* 8(3):293–303.

Clark, J. E., Cham, J. G., Bailey, S. A., Froehlich, E. M., Nahata, P. K., Full, R. J., and Cutkosky, M. R. 2001. Biomimetic design and fabrication of a hexapedal running robot. *IEEE International Conference on Robotics and Automation*, Seoul, Korea, May, p. 3643–3649.

Coleman, M. J., Chatterjee, A., and Ruina, A. 1997. Motions of a rimless spoked wheel: a simple three-dimensional system with impacts. *Dynamics and Stability of Systems* 12:139–159.

Full, R. J., Autumn, K., Chung, J. I., and Ahn, A. 1998. Rapid negotiation of rough terrain by the death-head cockroach. *American Zoologist* 38:81A.

Full, R. J., and Koditschek, D. E. 1999. Templates and anchors: Neuromechanical hypotheses of legged locomotion on land. *Journal of Experimental Biology* 202:3325–3332.

Gabrielli, G., and von Karman, T. H. 1950. What price speed? *Mechanical Engineering* 72:775–781.

Goldstein, H. 1980. *Classical Mechanics.* Reading, MA: Addison-Wesley.

Gregorio, P., Ahmadi, M., and Buehler, M. 1997. Design, control and energetics of an electrically actuated legged robot. *IEEE Transactions on Systems, Man, and Cybernetics* 27B(4):626–634.

Grimm, H. G. 1958. Animated toy. U.S. Patent No. 2827735.

Hirose, S. 1984. A study of design and control of a quadruped walking machine. *International Journal of Robotics Research* 3:113–133.

Honeywell, E. R. 1920. Walking tractor. U.S. Patent No. 1375752.

Huang, M. Z., and Waldron, K. J. 1990. Relationship between payload and speed in legged locomotion systems. *IEEE Transactions on Robotics and Automation* 6(5):570–577.

Kubow, T. M., and Full, R. J. 1999. The role of the mechanical system in control: A hypothesis of self-stabilization in hexapedal runners. *Philosophical Transactions of the Royal Society of London B* 354:849–862.

Mattel's Major Matt Mason's No. 6304 Space Crawler at http://www.wildtoys.com/MMMPage/MattelPlaysets/mmm3 part1.html.

National Science Foundation Institute for Mathematics and Its Application. Spring meeting, 1998. Available at http://www.ima.umn.edu/dynsys/spring/dynsys10.html.

Papadopoulos, D., and Buehler, M. 2000. Stable running in a quadruped robot with compliant legs. *IEEE International Conference on Robotics and Automation*, San Francisco, CA, April, pp. 444–449.

Pugh, D. R., Ribble, E. A., Vohnout, V. J., Bihari, T. E., Walliser, T. M., Patterson, M. R., and Waldron, K. J. 1990. Technical description of the adaptive suspension vehicle. *International Journal of Robotics Research* 9(2):24–42.

Raibert, M. H. 1986. *Legged Robots That Balance.* Cambridge, MA: MIT Press.

Saranli, U. 2000. SimSect hybrid dynamical simulation environment. Technical report, Computer Science Department, University of Michigan. Reference No. CSE-TR-436-00.

Saranli, U., Schwind, W. J., and Koditschek, D. E. 1998. Toward the control of a multi-jointed, monoped runner. *IEEE International Conference on Robotics and Automation*, Leuven, Belgium, May, pp. 2676–2682.

Schmitt, J., and Holmes, P. 2000. Mechanical models for insect locomotion I: Dynamics and stability in the horizontal plane. *Biological Cybernetics* 83:501–515.

Schwind, W. J., and Koditschek, D. E. 2000. Approximating the stance map of a 2-DOF monoped runner. *Journal of Nonlinear Science* 10:533–568.

Waldron, K. J., and Vohnout, V. J. 1984. Configuration design of the adaptive suspension vehicle. *International Journal of Robotics Research* 3(2):37–48.

Index to Multimedia Extensions

Extension	Media Type	Description
1	Video	RHex traversing simple outdoor obstacles
2	Video	RHex traversing a challenging indoor obstacle
3	Video	Front view of RHex over the rough surface obstacle
4	Video	Top view of RHex over the rough surface obstacle
5	Video	Example simulation with SimSect
6	Video	Demonstration of RHex's leg compliance
7	Video	Basic walking gait
8	Data	Power, speed, and specific resistance data and analysis scripts for all the experiments
9	Data	Data and analysis scripts for turning experiments
10	Video	RHex traversing a single high Styrofoam obstacle
11	Video	RHex traversing a composite obstacle
12	Data	Data and analysis scripts for the single obstacle experiments
13	Data	Data and analysis scripts for the composite obstacle experiments
14	Data	Data and analysis scripts for the rough surface experiments

NOTE: The multimedia extensions can be found online by following the hyperlinks from www.ijrr.org.